NOCICEPTOR NEURONS CONTROL POLLUTION-MEDIATED NEUTROPHILIC ASTHMA.

Jo-Chiao Wang [1], Theo Crosson [1], Amin Reza Nikpoor [2,3], Surbhi Gupta [3], Moutih Rafei [1], Sebastien Talbot [2,3,#]

[1] Department of Pharmacology and Physiology, University de Montreal, Canada
[2] Department of Physiology and Pharmacology, Karolinska Institutet, Sweden
[3] Department of Biomedical and Molecular Sciences, Queen's University, Canada

[#] Corresponding Author:
Sebastien Talbot, PhD
Phone: 438-521-3466
Email: *sebas.talbot@gmail.com; sebastien.talbot@queensu.ca; sebastien.talbot@ki.se*
ORCID: 0000-0001-9932-7174

ABSTRACT. The immune and sensory nervous systems, having evolved together, use a shared language of receptors and transmitters to maintain homeostasis by responding to external and internal disruptions. Although beneficial in many cases, neurons can exacerbate inflammation during allergic reactions, such as asthma. Our research modeled asthma aggravated by pollution, exposing mice to ambient $PM_{2.5}$ particles and ovalbumin. This exposure significantly increased bronchoalveolar lavage fluid neutrophils and γδ T cells compared to exposure to ovalbumin alone. We normalized airway inflammation and lung neutrophil levels by silencing nociceptor neurons at inflammation's peak using intranasal QX-314 or ablating TRPV1-expressing neurons. Additionally, we observed heightened sensitivity in chemical-sensing TRPA1 channels in neurons from pollution-exacerbated asthmatic mice. Elevated levels of artemin were detected in the bronchoalveolar lavage fluid from pollution-exposed mice, with artemin levels normalizing in mice with ablated nociceptor neurons. Upon exposure $PM_{2.5}$ particles, alveolar macrophages expressing pollution-sensing aryl hydrocarbon receptors, were identified as the source of artemin. This molecule enhanced TRPA1 responsiveness and increased neutrophil influx, providing a novel mechanism by which lung-innervating neurons respond to air pollution and suggesting a potential therapeutic target for controlling neutrophilic airway inflammation in asthma, a clinically intractable condition.

INTRODUCTION. Wildfire events and severity have increased significantly, with substantial adverse health impacts from wildfire-attributable (particulate matter) $PM_{2.5}$ exposure. The mortality burden from $PM_{2.5}$ exposure due to California fires from 2008 to 2018 was evaluated to ~53,000 premature deaths over the 11 years, resulting in an economic impact of $432 to $450 billion[1]. This form of asthma characterized by significant neutrophilic infiltration is often resistant to traditional treatments, highlighting a significant unmet need in respiratory healthcare[2]. Recent estimates suggest that neutrophilic asthma accounts for approximately 15-25% of all asthma cases, with around 50% of these cases being refractory to standard asthma treatments[3]. Taken together, resolving neutrophilic asthma constitutes an unmet clinical need of increasing importance.

Organisms have evolved complex fail-safe systems to maintain homeostasis, integrating mechanisms for threat detection, reflex responses, and tailored immune responses[4]. These functions are co-orchestrated by the immune and sensory nervous systems and designed to detect external threats and internal disturbances. To achieve this, both systems utilize shared metabolic pathways and a common signaling repertoire, including receptors, cytokines, and neuropeptides[5]. This shared molecular framework facilitates continuous interactions between these systems, which is crucial for regulating various processes. These include the physiological monitoring of barrier tissues such as skin[6], lung[7], and gut[8] and involve anticipatory immune responses[9] as well as the management of pathologies like allergic reactions[10,11], infections[12], and malignancies[13–16].

In lung disease, vasoactive intestinal peptide **(VIP**), released from a subset of pulmonary sensory neurons stimulated by the inflammatory cytokine IL-5, promotes allergic inflammation. It acts on $CD4^+$ T cells and resident innate lymphoid type 2 cells (**ILC2**s), increasing T helper type-2 (**T_H2**) cytokines, which are key drivers of asthmatic conditions[17,18]. Building on these findings, our research indicates that vagal nociceptor neurons contribute to airway hyperresponsiveness[4,19], mucus metaplasia[20,21], and sensing of immunoglobulin E and G[22,23]. These neurons also direct antibody class switching in B cells[24] and IgG production[25]. Our recent studies have revealed that a subset of nociceptor neurons is actively reprogrammed by asthma-driving cytokines IL-4/IL-13, making them sensitive to the inhibitory signal provided by NPY secreted by lung-innervating sympathetic neurons[26]. Additionally, we have discovered that lung-resident basophils sustain the pro-inflammatory phenotype of a population of vagal preceptors[27]. Other work shows that leukotriene C4 and IL-4 receptors, namely CysLTR2 and IL-4Rα, are associated with chronic itching and exacerbated bronchial contraction and inflammation in asthma[28].

Urban pollution and the increasing frequency and severity of wildfires contribute to higher concentrations of small particulate matter (less than 2.5 µm). This change shifts asthma from treatment-responsive eosinophilic and T_H2 types to treatment-resistant neutrophilic and mixed T_H17/T_H2 types. To address this unmet clinical need and explore whether

neuron silencing can alleviate this type of airway inflammation, we used a novel model of neutrophilic asthma. In this model, fine particulate matter (**FPM**) is added to ovalbumin. We also investigated the molecular mechanisms behind the heightened neuronal sensitivity observed in this context, identifying alveolar macrophages-produced artemin as a key driver of this hypersensitivity.

RESULTS. The group led by Prof. Ya-Jen Chang[29] has recently developed a novel method to model pollution-exacerbated asthma and to explore how fine particulate matter (**FPM**) causes airway inflammation. Their research demonstrates that FPM exposure triggers airway hyperreactivity (**AHR**) and neutrophilic inflammation, increases T_H1 and T_H17 immune responses, and elevates epithelial cell apoptosis rates. A key finding is that γδ T cells significantly contribute to this inflammation and AHR by producing IL-17A.

Building on this foundation, our team is investigating whether lung-innervating nociceptor neurons become sensitized during asthma exacerbations. To test this, male and female C57BL6 mice aged 6-10 weeks were sensitized with an emulsion of ovalbumin (OVA, 200 µg/dose) and aluminum hydroxide (1 mg/dose) on days 0 and 7 and later challenged intranasally with OVA (50 µg/dose) with or without fine particulate matter (FPM, 20 µg/dose) on days 14-16. JNC neurons were harvested on day 17, cultured for 24 hours, and then loaded with the calcium indicator Fura-2AM (**Fig. 1A**). Subsequent stimulation with the TRPA1 agonist AITC (10 µM) and the pan-neuronal activator KCl (40 mM) revealed increased neuronal responsiveness in mice exposed to the FPM and OVA combination compared to those exposed only to OVA. The latter showed similar sensitivity to the one of wild-type cells (**Fig. 1B-C**).

Building on recent findings that the asthma-promoting cytokines IL-4 and IL-13 reprogram lung-innervating nociceptor neurons to adopt a pro-allergic phenotype[26], we sought to understand how pollution-exacerbated asthma might reprogram these neurons. To do so, $TRPV1^{cre}$::td-$Tomato^{cre/wt}$ mice underwent the classic ovalbumin protocol with or without FPM exposure. $TRPV1^{+}$ JNC neurons were isolated, dissociated, and enriched to exclude adjacent satellite glial and immune cells, followed by FACS-sorting and RNA sequencing. Our data suggest the induction of several differentially expressed genes (DEGs) between OVA-FPM vs naïve groups (*Lifr, Oprm1*) (**Fig. 2A-B**), OVA-FPM vs OVA alone groups (*Oprm1, Nefh, P2ry1, Prkcb, Gabra1, Kcnv1*) (**Fig. 2C-D**), and OVA alone vs naïve groups (*Npy1r, Kcna1*) (**Fig. 2E-F**). Together, the induction of pollution-exacerbated asthma transcriptomically and functionally reprogram lung-innervating nociceptor neurons.

Building on this finding, we explore whether silencing these neurons affects pollution-exacerbated asthma. To test this, we adapted a neuron-blocking strategy, originally developed for pain and itch neurons, to silence tumor-innervating nociceptors. This approach utilizes non-selective ion channels (TRPA1 and TRPV1) as drug-entry ports for delivering a charged, membrane-impermeable form of lidocaine (QX-314). QX-314 enters sensory fibers during inflammation to block sodium currents, providing a targeted and durable (> 9h) electrical blockade of nociceptors without affecting immune cell function[30–33]. Intranasal injection of QX-314, a charged calcium channel blocker reversed allergic airway inflammation, coughing, mucus metaplasia, and hyperreactivity[18]. Here, we found that an acute intranasal dose of QX-314 at the peak of inflammation (day 17, 5 nmol, 50 µL) significantly reduced bronchoalveolar lavage fluid (BALF) eosinophil and neutrophil counts, normalizing these levels to the one observed in asthmatic mice (**Fig. 2A-B**). To substantiate these findings, we genetically engineered mice with either intact ($TRPV1^{wt}$::$DTA^{fl/wt}$) or ablated ($TRPV1^{cre}$::$DTA^{fl/wt}$) TRPV1-expressing nociceptor neurons[13,34,35]. Compared to controls, the ablated mice showed a marked reduction in BALF neutrophils and γδ T cells (**Fig. 2C-E**), confirming the significant role of nociceptors in modulating inflammation and immune responses in pollution-exacerbated asthma.

To further understand how nociceptor neurons regulate airway inflammation, we conducted an unbiased multiplex cytokine array. This analysis revealed elevated levels of asthma-driving cytokines IL-4 and IL-13, as well as the pro-inflammatory cytokines IL-6, CCL2, and TNFα, with TNFα levels normalizing following the ablation of nociceptor neurons (**Fig. 2F**). Additionally, targeted ELISA analysis showed increased levels of artemin, which returned to normal in the absence of nociceptor neurons (**Fig. 2G**). Artemin is a significant protein within the glial cell line-derived neurotrophic factor (GDNF) family, which is crucial for the development and functionality of the nervous system. Artemin is vital in developing sympathetic[36] and sensory neurons[37] by binding to the GFRα3-RET receptor complex on their surfaces, including many nociceptors. Activation of this receptor by artemin not only supports the survival and growth of these neurons during embryonic development but also leads to their increased sensitivity and hyperactivity under inflammatory conditions[38–40].

To better understand the role of artemin and its interactions in respiratory health, we focused on identifying the specific populations of vagal neurons that express the artemin receptor, Gfrα3. To achieve this, we conducted an in-silico analysis of single-cell RNA sequencing data from the jugular-nodose ganglion cells of Kupari (dataset GSE124312)[41]. This analysis revealed that *Gfra3* is expressed in several nociceptor neuron subtypes (**Fig. 3A-B**), specifically JG3 (OSM-R-expressing neurons), JG4 (TRPA1 and SSTR2-expressing), and JG6 (TRPM8-expressing).

In parallel, we explored the cellular sources of artemin and the aryl hydrocarbon receptor (AhR) using Immgen. Our analysis indicated high expression of the artemin gene (*Artn*) by macrophages, showing significant levels of AhR expression. However, slightly less than ILC2s and eosinophils (**SF. 1**). Based on these in silico findings, we harvested alveolar macrophages from naïve C57BL/6 mice and exposed them to fine particulate matter (FPM). This resulted in time-dependent increases in *Artn* transcript expression, underscoring the dynamic response of these cells to environmental stimuli (**Fig. 3C-D**). These findings elucidate significant cellular interactions involving artemin and AhR, highlighting their roles in inflammation and potentially in the pathophysiology of respiratory diseases.

A recent study has linked the overexpression of artemin with increased mRNA levels of several key nociceptor neurons inflammation markers including *Gfrα3, TrkA, Trpv1,* and *Trpa1*, which was associated with the enhancement of thermal sensitivity in mice by lowering heat thresholds and amplifying responses to thermal stimuli[39]. Building on this, our investigations into FPM-sensitized neurons revealed heightened calcium responses to the TRPA1 agonist AITC (**Fig 1B-C**), suggesting a potential role for artemin in this enhanced activity. Subsequent experiments conducted with naïve C57BL/6 mice provided further evidence; JNC neurons from these mice demonstrated increased AITC responses compared to those treated with a vehicle (**Fig 1F-H)**. These findings collectively suggest that alveolar macrophages, by releasing artemin, act as an upstream mediator sensitive to pollutants. This mechanism leads to sensitizing nociceptor neurons, facilitating their role in upregulating allergic airway inflammation. This pathway underscores a critical interaction between environmental pollutants and the neurogenic exacerbation of allergic responses (**SF 2**).

DISCUSSION. Our research, along with others, indicates that nociceptor neurons typically promote regulatory immunity in the context of bacterial[42], viral[43], fungal[44] infections, or malignancies[13]. To our knowledge, the impact of neuro-immunity in regulating T_H17 immunity is more limited, with only one study showing that TRPV1$^+$ neuron activation elicits a local type 17 immune response that augmented host defense to C. albicans and S. aureus[9]. Given the knowledge gap in lung inflammation, we set out to assess how neuro-immunity shapes neutrophil influx and T_H17/T_H2 activation in a model of pollution-exacerbated airway inflammation. We found that ablation or silencing of nociceptor neurons prevented the induction of airway inflammation, highlighting a potential novel therapeutic pathway for treating refractory asthma. This finding phenocopy our previous preclinical data showing that nociceptor neuron silencing using a charged voltage-gated sodium channel[18,24,30] or calcium channel[31] blocker can stop eosinophilic airway inflammation. It also matches the absence of effect we found in nociceptor neuron ablation in a model of T_H1 inflammation induced by CFA/OVA[17].

Dissecting lung neuro-immunity.
Chiu's group demonstrated that during bacterial infections, nociceptor neurons limit neutrophil influx and their antimicrobial activity by releasing the neuropeptide CGRP[12]. In support of this, Ugolini's team found that ablating $Na_V1.8^+$ nociceptor neurons during HSV-1 viral infections led to a significant increase in neutrophils in the skin, associated with heightened cytokine production and viral skin lesions[43]. Here, we report that ablating TRPV1 neurons, a subset of $Na_V1.8$-expressing sensory neurons, decreases the influx of neutrophils exacerbated by pollution, suggesting a different underlying mechanism, likely involving substance P rather than CGRP.

Thus, we showed that vagal nociceptor neurons can detect immune complexes formed between allergens and IgE, triggering the release of substance P (SP) and vasoactive intestinal peptide (VIP) but not CGRP[22]. We confirmed these findings in asthmatic mice's bronchoalveolar lavage fluid (BALF)[24]. Further, we demonstrated that SP promotes mucus metaplasia in the lungs of asthmatic mice[20] and influences B cell antibody class switching[24]. Other researchers corroborated both findings[25,45–47]. Additionally, we observed that TRPV1$^+$ nociceptor neuron ablation impairs antigen trafficking in lymph nodes[48], and antibody class-switching[25] potentially reducing the severity or development of allergic reactions[49].

Emerging research highlights the varied immunomodulatory effects of different neuropeptides. For instance, CGRP hinders the migration of dendritic cells in psoriasis[11,50], whereas SP enhances their migration to lymph nodes in atopic dermatitis[10]. VIP and neuromedin U (NMU) increase the production of pro-asthmatic cytokines by lung ILC2 cells[18,51–54], whereas CGRP has similar[55,56] or opposite effect[57]. In the lungs, CGRP reduces the infiltration of neutrophils and gamma-delta T (γδT) cells, offering protection against Staphylococcus aureus pneumonia[58,59]. Conversely, CGRP can worsen psoriasis in the skin by inducing dendritic cells to produce IL-23, which activates IL-17-producing γδT cells, exacerbating inflammation[44]. In response to C. albicans, sensory neurons also release CGRP, prompting CD301b$^+$ dendritic cells to produce IL-23 and initiating a T helper type-17 (T_H17) and γδT cell-mediated response marked by IL-17A and IL-22 production, which enhances host resistance to infection[9]. Our findings indicate that nociceptor neuron ablation reduces γδ T-cell activation, an effect we attribute to SP/VIP-driven responses due to our model's lack of heighten CGRP release[18,24]. Future research will focus on how neurons directly regulate γδ T-cell and neutrophil function in these contexts.

Aryl hydrocarbon receptor and alveolar macrophages
The aryl hydrocarbon receptor (AhR) is essential in modulating inflammation, as evidenced by its ability to decrease

inflammation in the skin of psoriasis patients[60]. Mice lacking AhR display worsened symptoms, underscoring its vital role in controlling inflammation[61]. Beyond its expression in alveolar macrophages, as we observed, AhR is also present in various other innate immune cells such as ILC2, eosinophils, and neurons. A recent preprint highlights AhR's dual function as a critical molecular sensor and regulator, balancing neural protection and axon regeneration[62]. It shows that while AhR activation in DRG sensory neurons inhibits axon regeneration, its deletion activates gene programs associated with axonogenesis, reduces inflammation and stress signaling, and enhances pro-growth pathways following peripheral axotomy[62]. AhR has also been implicated in regulating the gut-brain axis[63]. Although we have not formally tested this, it is plausible that AhR-expressing neurons, similar to alveolar macrophages, can directly sense fine particulate matter (FPM), potentially explaining the direct neuronal reprogramming we observed after pollutant exposure. Future research will explore this hypothesis using nociceptor neurons with conditional AhR knockout.

Artemin sensing, TRPA1 sensitization, and airway inflammation.
Alveolar macrophages serve as an early warning system in the lungs[64]. We found that they detect pollutants like fine particulate matter and trigger defensive reflexes by releasing artemin. This action activates and sensitizes nociceptor neurons to TRPA1-sensing noxious stimuli. Single-cell RNA sequencing revealed that a subtype of TRPA1, SST2R neurons, express the GDNF receptor GFRα3 and are sensitized by artemin. This finding complements previous research showing that keratinocyte-produced TSLP sensitizes skin-innervating nociceptor neurons, promoting itch and skin atopy[65]. In the lungs, TRPA1 germline knockout reduces allergic airway inflammation[66,67], while Genentech's recent Phase 1 research demonstrated that TRPA1 agonists are elevated in asthmatic human airways and contribute to inflammation and hyperreactivity. Their development of GDC-0334, a selective TRPA1 antagonist, effectively reduces inflammation, cough, and allergic reactions in preclinical trials and decreases pain and itch in human studies[68], supporting TRPA1 sensitization and nociceptor neuron as a whole as a major upstream asthma driver.

We previously observed that neurons in the nodose ganglia express high levels of TRPA1 and exhibit increased thermal sensitivity and neuron outgrowth in response to brain-derived neurotrophic factor (BDNF) yet remain unresponsive to nerve growth factor[35]. Here, we showed that lung-innervating vagal neurons express GFRa3 and respond to artemin, which sensitizes TRPA1 responses and promotes subsequent airway inflammation. JNC neurons show significant transcriptomic reprogramming when exposed to ovalbumin plus fine particulate matter (OVA+FPM), like their response to pro-asthmatic cytokines. Previous studies support this reprogramming and TRPA1 sensitization. Among others, data shows that EGR1 and artemin levels are elevated in atopic dermatitis patients, where EGR1-deficient mice showed reduced nerve density and scratching behavior mediated by artemin signaling[69]. Overexpression of artemin also increases the sensitivity of sensory neurons to thermal stimuli[39], highlighting its crucial role in regulating neuronal outgrowth and sensitivity in atopic conditions. Taking together, preventing artemin's action on neurons by blocking GFRa3 might also reveal novel therapeutic targets to avoid the maladaptive involvement of nociceptor neurons in pollution-exacerbated asthma.

In the context of pollution-exacerbated asthma, our research links the sensitization of TRPA1^{+} nociceptor neurons and heightened allergic inflammation to artemin produced by macrophages. We propose new therapeutic targets to dampen neutrophilic airway inflammation by i) targeting the AhR-mediated pollution sensing by alveolar macrophages (AM), ii) inhibiting artemin's effect on neurons by blocking GFRa3, iii) blocking TRPA1 using novel antagonists such as GDC-0334, and iv) silencing nociceptor neurons with charged lidocaine derivatives.

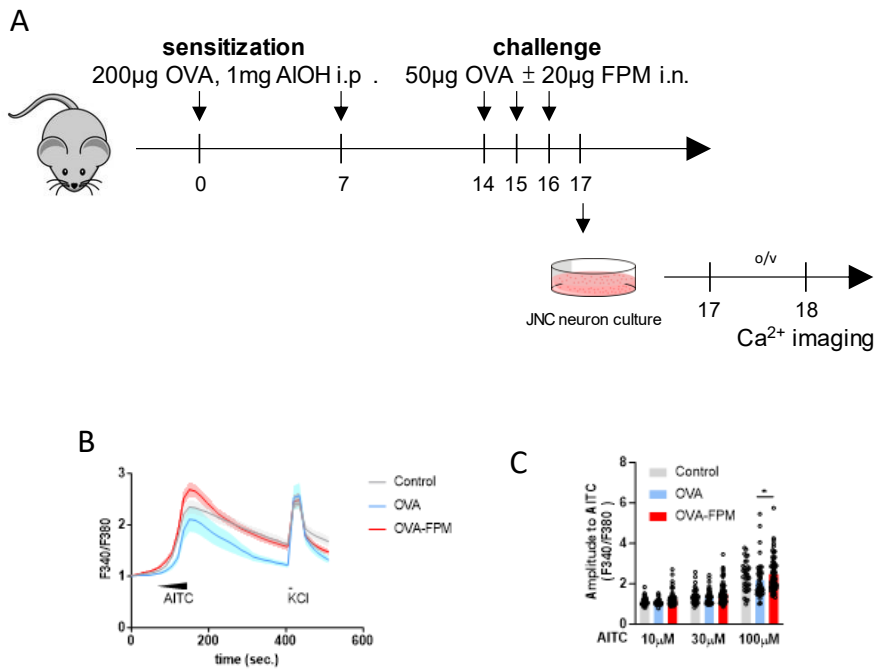

Figure 1. Air pollution exacerbates nociceptor neurons' activity.

(**A-C**) Male and female C57BL6 mice aged 6-10 weeks were sensitized via intraperitoneal injection with an emulsion containing ovalbumin (OVA, 200 µg/dose) and aluminum hydroxide (1 mg/dose) on days 0 and 7. They were then challenged intranasally with OVA (50 µg/dose) with or without fine particulate matter (FPM, 20 µg/dose) on days 14-16. Bronchoalveolar lavage fluid (BALF) was collected, and JNC neurons were cultured on day 17. (**B-C**) JNC neurons were harvested and cultured for 24 hours. Following culturing, the cells were loaded with the calcium indicator Fura-2AM and sequentially stimulated with AITC (10 µM at 60-90 seconds, 30 µM at 90-120 seconds, 100 µM at 120-150 seconds) and KCl (40 mM at 420-435 seconds). Calcium flux was recorded throughout these stimulations (**B**), and the amplitude of AITC responses was calculated as the ratio of peak F340/F380 after stimulation to the baseline F340/F380 30 seconds before stimulation (**C**).

*Data are presented as means ± 95% CI (**B**), means ± SEM (**C**)*

*(**B-C**) Representative data from 2 independent experiments. AITC-responsive neurons were included in amplitude analysis. n=35 neurons from control mice, n=42 neurons from OVA-treated mice, and n=76 neurons from OVA-FPM-treated mice were analyzed.*

*Statistical significance is indicated by *p≤0.05, **p≤0.01, ***p≤0.001, ****p≤0.0001.*

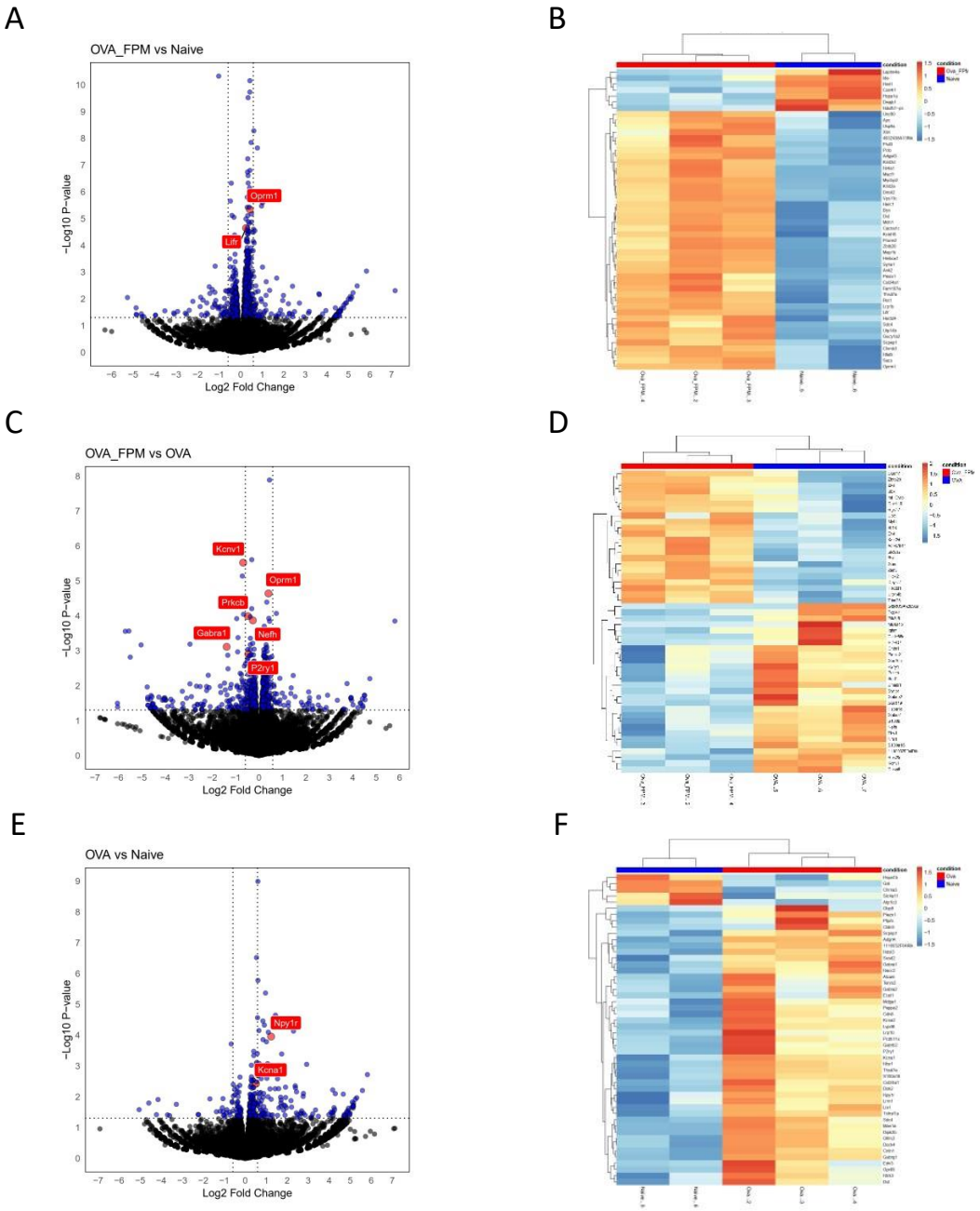

Figure 2. Air pollution reprogram nociceptor neurons' transcriptome.

(**A-F**) Naïve male and female TRPV1^{cre}::td-Tomato$^{cre/wt}$ mice, aged 6-10 weeks, were subjected to either a pollution-exacerbated asthma protocol, the classic ovalbumin (OVA) protocol, or were kept naïve. On day 17, at the peak of inflammation, JNC neurons were harvested, dissociated, TRPV1^{+} neurons FACS-purified (td-tomato+) from stromal cells and non-peptidergic neurons, and isolated for RNA sequencing.

Differentially expressed genes were calculated and displayed as volcano plots and heatmaps for the comparisons: OVA-FPM vs. naïve (**A-B**), OVA-FPM vs. OVA (**C-D**), OVA alone vs. naïve (**E-F**). Significant neuronal reprogramming was observed and characterized by the overexpression in the OVA-FPM vs. naïve groups (Lifr, Oprm3), OVA-FPM vs. OVA alone groups (Oprm1, Nefh, P2ry1, Prkcb, Gabra1, Kcnv1), and OVA alone vs. naïve groups (Npy1r, Kcna1).

*Data are presented as volcano plot ($p < 0.05$; **A, C, E**) or heatmap (**B, D, F**) showing normalized gene expression (log_2 (0.01 + transcripts per million reads (TPM)) − mean).*

The sequencing experiment was not repeated.

n consisted of 2-3 mice.

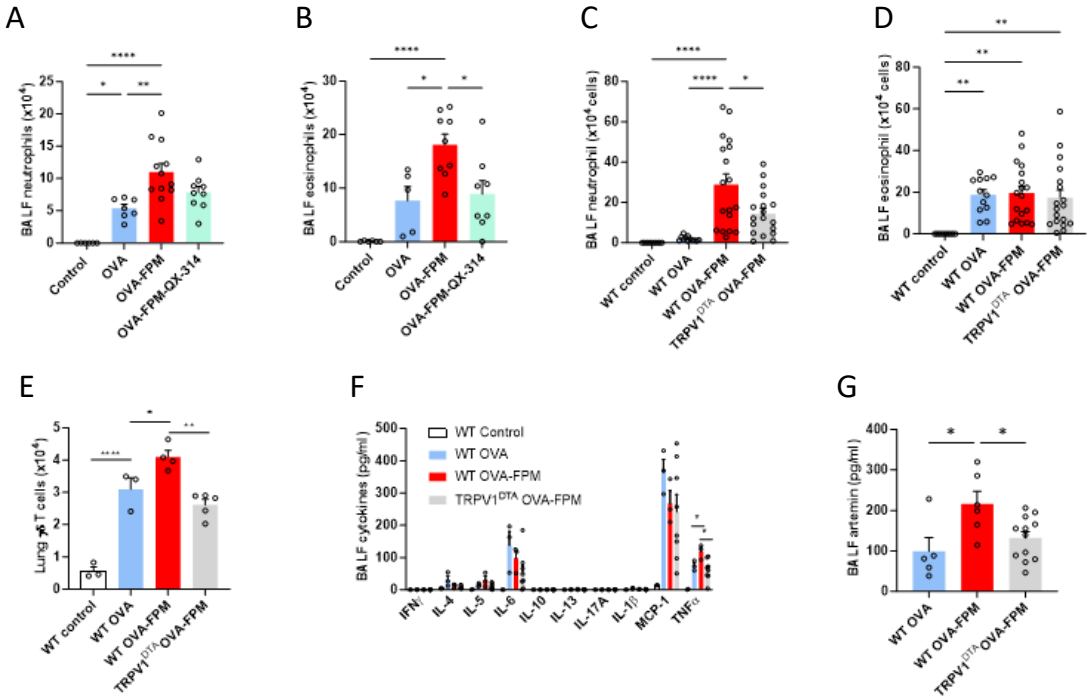

Figure 3. Nociceptor neurons control pollution-exacerbated asthma.

(**A-B**) Male and female C57BL6 mice aged 6-10 weeks were sensitized via intraperitoneal injection with an emulsion containing ovalbumin (200 µg/dose in 100 µl) and aluminum hydroxide (1 mg/dose in 100 µl) on days 0 and 7. They were then challenged intranasally with OVA (50 µg/dose in 50 µl) with or without fine particulate matter (FPM, 20 µg/dose in 50 µl) on days 14-16 and received intranasal injections of QX-314 (5 nmol/dose in 50 µl) on day 16, 30 minutes after the last challenge. Bronchoalveolar lavage fluid (BALF) was collected on day 17 and analyzed immune influx immunophenotyped by flow cytometry. Compared to naïve mice or OVA-exposed mice, the one co-challenged with OVA-FPM showed increased BALF infiltration of neutrophils (**A**) and eosinophils **(B**). The mice treated with QX-314 were protected from these increases (**A-B**).

(**C-G**) Male and female littermate control (TRPV1^{wt}::DTA$^{fl/wt}$) and nociceptor ablated (TRPV1^{cre}::DTA$^{fl/wt}$) mice aged 6-10 weeks were sensitized via intraperitoneal injection with an emulsion containing ovalbumin (OVA, 200 µg/dose) and aluminum hydroxide (1 mg/dose) on days 0 and 7. They were then challenged intranasally with OVA (50 µg/dose) with or without fine particulate matter (FPM, 20 µg/dose) on days 14-16. Bronchoalveolar lavage fluid (BALF) was collected on day 17, and immune influx was immunophenotyped by flow cytometry.

Compared to naïve mice or OVA-exposed mice, the one co-challenged with OVA-FPM showed increased BALF infiltration of neutrophils (**C**) and γδ T-cells (**E**). The nociceptor ablated (TRPV1^{cre}::DTA$^{fl/wt}$) mice were protected from these increases (**C, E**) but showed similar levels of BALF eosinophils (**D**).

(**F-G**) BALF cytokines were measured using a cytokine multiplex array and ELISA, and increased levels of IL-5, MCP1 (CCL2), TNFα, and artemin were found. TNFα (**F**) and artemin (**G**) rise were absent in nociceptor-ablated mice.

*(**A-G**) Data are presented as means ± SEM.*

*(**A-B**) Pooled data from 2 independent experiments. n=6-12 mice per group. (**C-E**) Pooled data from 2 independent experiments. n=9-18 mice per group. (**F**) Representative data from 2 independent experiments. n=3-6 mice per group. (**G**) Representative data from 2 independent experiments. n=2-8 mice per group. (**J**) Pooled data from 2 independent experiments. n=5-12 mice per group.*

*Statistical significance is indicated by *p≤0.05, **p≤0.01, ***p≤0.001, ****p≤0.0001.*

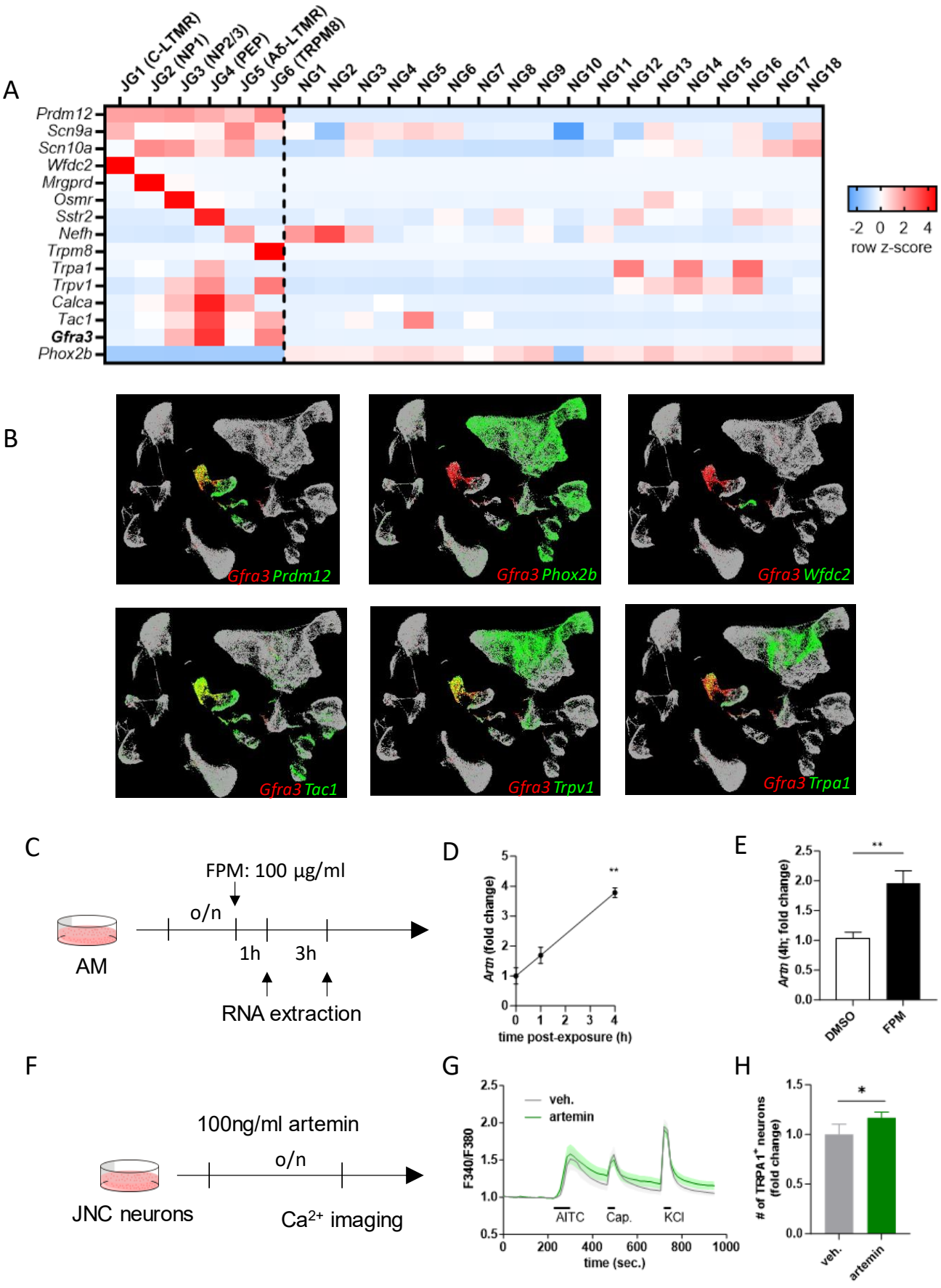
A
JG1 (C-LTMR)
JG2 (NP1)
JG3 (NP2/3)
JG4 (PEP)
JG5 (Aδ-LTMR)
JG6 (TRPM8)
NG1
NG2
NG3
NG4
NG5
NG6
NG7
NG8
NG9
NG10
NG11
NG12
NG13
NG14
NG15
NG16
NG17
NG18
Prdm12
Scn9a
Scn10a
Wfdc2
Mrgprd
Osmr
Sstr2
Nefh
Trpm8
Trpa1
Trpv1
Calca
Tac1
Gfra3
Phox2b
-2 0 2 4
row z-score
B
Gfra3 Prdm12
Gfra3 Phox2b
Gfra3 Wfdc2
Gfra3 Tac1
Gfra3 Trpv1
Gfra3 Trpa1
C
FPM: 100 µg/ml
o/n
AM
1h
3h
RNA extraction
D
Arm (fold change)
time post-exposure (h)
E
Arm (4h; fold change)
DMSO
FPM
F
100ng/ml artemin
o/n
JNC neurons
Ca2+ imaging
G
veh.
artemin
F340/F380
AITC
Cap.
KCl
time (sec.)
H
# of TRPA1+ neurons (fold change)
veh.
artemin

Figure 4. Artemin sensitizes TRPA1 activity in vagal sensory neurons.

(**A**) In-silico analysis of the dataset GSE124312 generated a heatmap showing the transcript expression levels of the pan neural-crest lineage transcription factor (*Prdm12*), voltage-gated sodium channels (*Scn9a, Scn10a*), jugular subset markers (*Wfdc2, Mrgprd, Osmr, Sstr2, Nefh, Trpm8*), peptidergic neuron markers (*Trpa1, Trpv1, Calca, Tac1, Gfra3*), and the pan placodal lineage marker (Phox2b). Experimental details and cell clustering are defined in Kupari et al.[41].

(**B**) In-silico analysis of GSE192987 presenting the co-expression of Gfra3 with TRPA1 or other inflammatory markers. The data are presented as a heatmap displaying the row z-scores (A) or cells that has TPTT>1 in UMAPs.

(**C-E**) Alveolar macrophages from naïve male and female C57BL6 mice (3 x 10^5 cells/well) were cultured overnight and stimulated with DMSO or FPM (100 µg/ml). RNA was extracted at 1 and 4h post-stimulation, and *Artn* expression was analyzed using qPCR (**C**). Data showed that FPM increased artemin transcript expression 1 and 4h post-stimulation (**D-E**).

(**F-H**) JNC neurons were harvested, pooled, and cultured overnight with either vehicle or artemin (100 ng/mL). The cells were then sequentially stimulated with AITC (TRPA1 agonist; 300 µM at 240-270 seconds), capsaicin (TRPV1 agonist; 300 nM at 320-335 seconds), and KCl (40 mM at 720-735 seconds). The percentage of AITC-responsive neurons among KCl-responsive cells was normalized to the vehicle-treated dish from each batch of experiments (**F**). Artemin-exposed neurons showed increased responsiveness to AITC, while the responses to capsaicin and KCl were not impacted (**G-H**).

*Data are presented as heatmap (**A**), TSNe plot (**B**), means ± SEM (**D, E, H**) or means ± 95% CI of the maximum Fura-2AM (F/F0) fluorescence recorded every 15 seconds (**G**).*

*(**D**) Data from 1 experiment with n=2 technical repeats. (**E**) Pooled data from 2 independent experiments with n=8 technical repeats. (**G**) Representative data from 2 independent experiments with n=107 vehicle-treated and n=122 artemin-treated neurons were analyzed. (**H**) Pooled data from 2 independent experiments with n=4 fields of view per group.*

*Statistical significance is indicated by *p≤0.05, **p≤0.01, ***p≤0.001, ****p≤0.0001.*

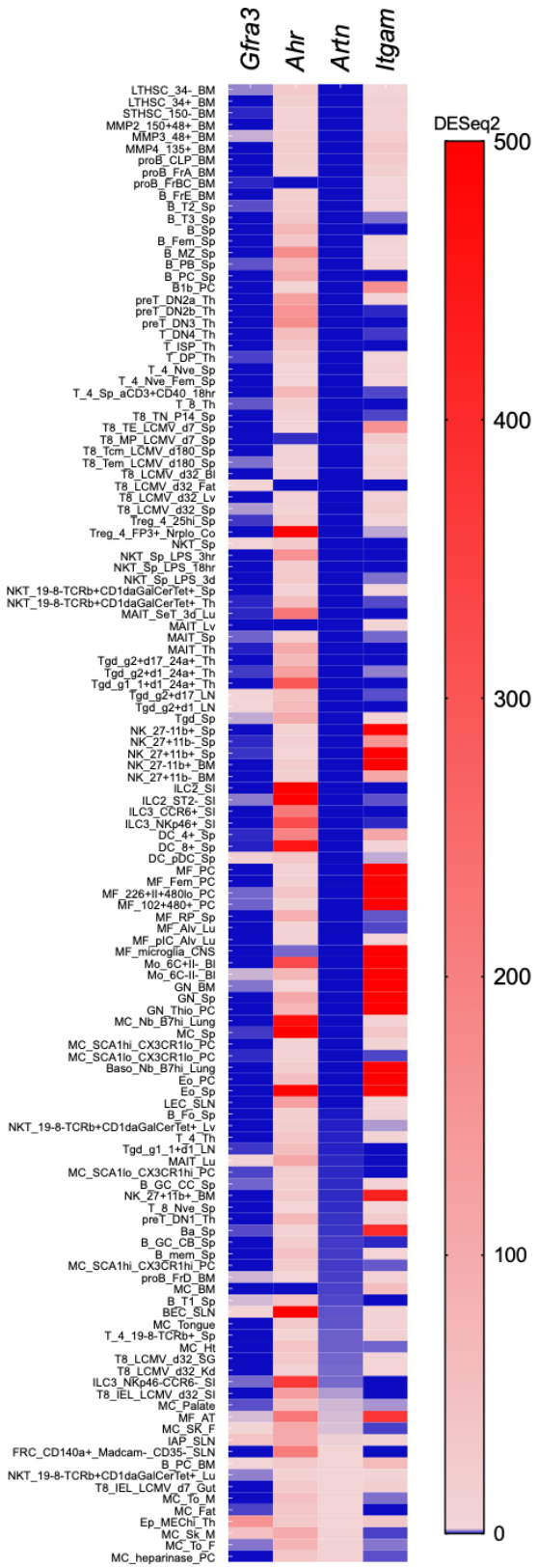

Supplementary figure 1. In silico analysis of Artn expression in mouse immune cells

In silico analysis of Artn expression in mouse using the Immgen database[70].

Data are presented as per-gene z-scores of normalized gene expression using the median of ratios method.

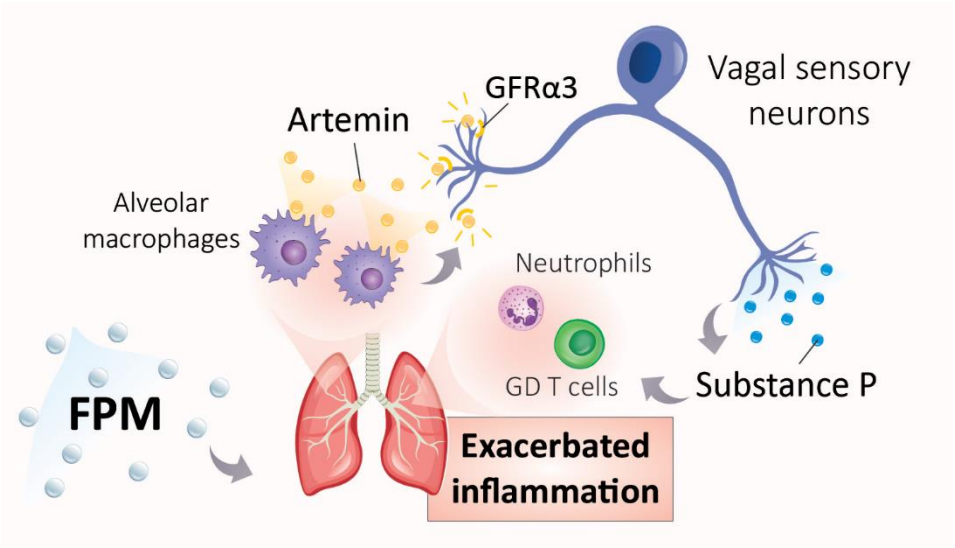

Supplementary figure 2. Schematic of nociceptor involvement in air pollution-exacerbated allergic asthma.

In our study, we modeled pollution-exacerbated asthma in mice by exposing them to $PM_{2.5}$ particles and ovalbumin. This exposure significantly increased bronchoalveolar lavage fluid (BALF) neutrophils and γδ T-cells compared to exposure to ovalbumin alone. To address the heightened airway inflammation, we applied intranasal QX-314, a charged derivative of lidocaine, during peak inflammation, which effectively normalized the inflammation. Similarly, ablating TRPV1-expressing nociceptor neurons also normalized lung neutrophil levels.

Further analysis using calcium microscopy on neurons from the jugular-nodose complex showed increased sensitivity of TRPA1 channels in neurons from pollution-exacerbated asthmatic mice. Elevated TNFα and the growth factor artemin levels were found in the BALF of pollution-exposed mice, which normalized following nociceptor neuron ablation.

We pinpointed alveolar macrophages as the source of artemin, which, expressing aryl hydrocarbon receptors, responded to fine particulate matter (FPM) by releasing artemin. This release increased TRPA1 responsiveness to its agonist, mustard oil, exacerbating airway inflammation. Our findings indicate that silencing nociceptor neurons can interrupt this mechanistic pathway and offer a novel approach to mitigating neutrophilic airway inflammation in pollution-driven asthma.

MATERIALS AND METHODS

Animals and in vivo experiments

All procedures involving animals adhered to the guidelines of the Canadian Council on Animal Care (CCAC) and the Queen's University Animal Care Committee (UACC). Mice were accommodated in individually ventilated cages with free water and food access under 12-hour light cycles. The strains used, C57BL6/J (000664), $DTA^{fl/fl}$ (010527), and $TRPV1^{cre}$ (017769), were obtained from the Jackson Laboratory and bred in-house.

For the ovalbumin (OVA)-induced allergic airway inflammation model, C57BL6 mice were sensitized via intraperitoneal injection with a mix of grade V OVA (200 µg/dose; Sigma-Aldrich A5503) and Imject® Alum (1 mg/dose; ThermoFisher 77161) on days 0 and 7. Subsequently, they underwent intranasal challenges with OVA (50 µg/dose), with or without fine particulate matter (FPM; 20 µg/dose; NIST 2786), from day 14 to 16. Control mice were sensitized but not challenged. The mice were euthanized on day 17, and samples from bronchoalveolar lavage fluid, lung tissue, and the jugular-nodose complex (JNC) were collected.

Bronchoalveolar lavage

Bronchoalveolar lavage was performed on mice anesthetized using previously described tracheal incision methods. The mice underwent lavage twice with 1 ml of either PBS or FACS buffer (2% FBS and one mM EDTA in PBS) utilizing a Surflo ETFE IV Catheter 20G x 1" (Terumo Medical Products SR-OX2025CA). The lavage fluid was then centrifuged at 350 x G for 6.5 minutes. The supernatant was collected for ELISA analysis, while the cell pellets were resuspended, treated with RBC lysis solutions (Cytek TNB-4300-L100 or Gibco A1049201), and stained for surface markers for subsequent flow cytometry analysis.

Lung tissues were harvested after the diaphragm incision, and transcardial perfusion was performed with 10 ml of PBS. The tissues were then finely minced using razor blades and collected either into TRIzol™ Reagent (Invitrogen 15596026) for RNA extraction or into a digestion buffer containing 1.6 mg/ml collagenase type 4 (Worthington LS004189) and 100 µg/ml DNase I (Roche 11284932001) in supplemented DMEM for the preparation of a single-cell suspension. This suspension was achieved through 45 minutes of enzymatic digestion at 37°C. Mechanical dissociation was carried out using 18-gauge needles halfway through the digestion period (30 minutes), then straining through a 70 µm nylon mesh and RBC lysis. For flow cytometry or fluorescence-activated cell sorting (FACS), the cells were resuspended in FACS buffer; for in vitro stimulation, the cells were resuspended in FBS-supplemented DMEM, seeded into 96-well plates and cultured at 37°C with 5% CO2 for the designated time before collecting the supernatant.

Alveolar macrophage culture

Alveolar macrophages were isolated from the bronchoalveolar lavage fluid (BALF) of naïve mice, with these cells constituting approximately 95% of the sample. The cells were centrifuged and treated with RBC lysis as previously described, then cultured overnight at a density of 3 x 10^5 cells per well in 96-well plates. The culture medium used was DMEM (Gibco 11965092) supplemented with one mM sodium pyruvate (Gibco 11360070), two mM GlutaMAX™ (Gibco 35050061), 100 U/mL penicillin and 100 µg/mL streptomycin (Corning 30-002-CI), ten mM HEPES (Gibco 15630080), and 10% FB Essence (VWR 10805-184).

The cells were then stimulated with 100 µg/ml fine particulate matter (FPM; NIST 2786) for 1-4 hours. Following stimulation, RNA was extracted for quantitative PCR (qPCR) analysis.

Neuron culture

The jugular-nodose complex (JNC) was collected after exsanguinating anesthetized mice. The ganglia were placed into a digestion buffer composed of 1 mg/ml (325 U/ml) collagenase type 4 (Worthington LS004189), 2 mg/ml (1.8 U/ml) Dispase II (Sigma 04942078001), and 250 µg/ml (735.25 U/ml) DNase I (Roche 11284932001), prepared in supplemented DMEM media without FB Essence. This mixture was incubated at 37°C for 60 minutes to facilitate enzymatic digestion. Mechanical dissociation was then performed by repeatedly pipetting the digested tissue with pipette tips of decreasing diameter, concluding with 25-gauge needles. This was followed by density gradient centrifugation at 200 g for 20 minutes, with low acceleration and deceleration settings, using a layer of 150 mg/ml bovine serum albumin (BSA; Hyclone SH30574.02) in a PBS solution.

The cells at the bottom were collected, RBC lysed, and then seeded onto glass-bottom dishes (ibidi 81218) pre-coated with 50 µg/ml laminin (Sigma L2020) and 100 µg/ml poly-D-lysine (Sigma P6407). They were cultured overnight in Neurobasal-A media (Gibco 10888022) supplemented with one mM sodium pyruvate (Gibco 11360070), two mM GlutaMAX™ (Gibco 35050061), 100 U/mL penicillin, 100 µg/mL streptomycin (Corning 30-002-CI), ten mM HEPES (Gibco 15630080), B-27 supplement (Gibco 17504-044), 50 ng/ml mouse nerve growth factor (NGF; Gibco 13257-019), two ng/ml mouse glial-derived neurotrophic factor (GDNF; Novus NBP2-61336), and cytosine-β-D-arabinofuranose (Thermo Scientific J6567106). In some experiment, 100 ng/ml artemin or 50 M HCl (as vehicle control) were treated *in*

vitro to dishes, without NGF or GDNF supplements. This setup was used for subsequent calcium imaging recordings.

Calcium imaging recording

Cultured neurons were loaded with the calcium indicator dye, five µM fura-2 AM (Cayman Chemical Company 34993), and incubated at 37°C for 40 minutes. Following incubation, the neurons were washed four times with standard external solution (SES; Boston BioProducts C-3030F) before imaging in the same solution. The data captured from the Fura-2 signals were utilized for further analysis. Agonists, diluted in SES, were administered using a ValveLink8.2 system (AutomateScientific) equipped with 250 µm Perfusion Pencil® tips (Automate Scientific) and controlled via Macro Recorder (Barbells Media, Germany). To ensure complete drug washout, SES continuously flowed between drug injections.

Imaging for Fura-2 experiments was performed using an S Plan Fluor ELWD 20X objective lens (NIKON) to enhance UV light transmission. In contrast, GcaMP6f experiments employed an S Plan Fluor LWD 20X lens (NIKON) to achieve improved resolution. Images were captured every 3 or 4 seconds using sCMOS cameras, including pco. Edge 4.2 LT (Excelitas Technologies), Prime 95B (Teledyne Photometrics), and Orca Flash 4.0 v2 (Hamamatsu Photonics). All imaging activities were conducted on ECLIPSE Ti2 Inverted Microscopes (NIKON).

Regions of interest (ROI) were manually delineated using NIS-Elements software (NIKON), and the F340/F380 ratios were exported to Excel (Microsoft) for further analysis. Data were condensed into a maximum value every 15 seconds for all analyses.

Flow cytometry

Single-cell suspensions derived from bronchoalveolar lavage fluid (BALF) or lung samples were stained with Ghost Dye Violet 510 (Cytek, 13-0870-T100) and antibody cocktails in PBS. The cells were incubated at four °C for 30 minutes, followed by fixation with 10% neutral buffered formalin (Sigma Aldrich, HT501128) at room temperature for 15 minutes before acquiring flow cytometry data. For the assessment of eosinophil and neutrophil infiltration, BALF cells were stained with fluorochrome-conjugated antibodies targeting CD45 (30-F11), CD90.2 (53-2.1), CD11b (M1/70), CD11c (N418), Ly6C (HK1.4), Ly6G (1A8), and Siglec-F (1RNM44N). For the analysis of γδ T cells in lung cells, the staining involved CD45 (30-F11), TCRγδ (GL3), CD90.2 (53-2.1), and lineage markers including TCRβ (H57-597), CD19 (1D3/CD19), NK1.1 (PK136), CD11b (M1/70), CD11c (N418), F4/80 (BM8), and FcεRIα (MAR-1), sourced from Biolegend or Thermo Fisher Scientific. Data was acquired using a FACS Canto II (BD Biosciences).

Real-time quantitative PCR (qPCR)

Stimulated alveolar macrophages were lysed using TRIzol Reagent and stored at -80°C before RNA extraction. RNA from sorted cells was extracted using the PureLink RNA Micro Scale Kits (ThermoFisher, 12183016), while RNA from lung tissues or lung cell suspensions was extracted with the E.Z.N.A.® Total RNA Kit I (Omega Bio-tek®, R6834). All RNA extractions followed the manufacturer's instructions, including phenol-chloroform phase-based purification and mixing with equal volumes of isopropanol.

cDNA synthesis was conducted using SuperScript VILO Master Mix (Invitrogen, 11755050), utilizing 1-2 µg of RNA as a template for each reaction. Quantitative polymerase chain reaction (qPCR) was carried out with PowerUp SYBR Green Master Mix (Applied Biosystems, A25742), using 50-100 ng of cDNA templates and 200 nM of respective primers. The qPCR was executed on a Mic qPCR Cycler (Bio Molecular Systems) or a CFX Opus Real-Time PCR System (Bio-Rad Laboratories). The primer pair used for the *Artn* gene was forward TGATCCACTTGAGCTTCGGG and reverse CTCCATACCAAAGGGGTCCTG.

Enzyme-linked immunosorbent assay (ELISA)

artemin in BALF is determined by ELISA (R&D system DY1085-05) according to the manufacturer's manual. Inflammatory cytokines in BALF were detected by Cytometric Beads Array Flex Sets purchased from BD Biosciences: Master Buffer Set (558266), IL-1β (560232), IL-4 (558298), IL-5 (558302), IL-6 (558301), IL-10 (558300), IL-13 (558349), IL-17A (560283), IFNγ (558296), MCP-1 (558342), and TNF (558299) according to the manufacturer's manual.

In silico analysis of RNA-Seq data

Data were extracted from Kupari et al.'s supplementary materials, with clusters defined according to the original publication[41]. Bulk JNC sequencing was analyzed with DESeq2. Immgen data were extracted as csv and plotted with GraphPad Prism. Data from single-cell portal was extracted and plotted with R.

Data availability

Information and raw data are available from the lead contact upon reasonable request. (GEO pending)

Statistics

P *values ≤ 0.05* were considered statistically significant. One-way ANOVA, two-way ANOVA, and Student t-tests were performed using GraphPad Prism. DESeq2 and Seurat analysis and statistics were performed using RStudio.

Replicates

Replicates (n) are described in the figure legends and represent the number of animals for *in vivo* data. For *in vitro* data, replicates can either be culture wells or dishes, animals, fields-of-view (microscopy), or neurons (calcium microscopy), but always include different preparations from different animals to ensure biological reproducibility.

DECLARATIONS OF COMPETING OF INTEREST. The authors declare that there are no conflicts of interest.

ACKNOWLEDGEMENTS. ST work is supported by the Canadian Institutes of Health Research (CIHR; 407016, 461274, 461275), Canadian Foundation for Innovation (44135), Canadian Cancer Society Emerging Scholar Research Grant (708096), Knut and Alice Wallenberg Foundation (KAW 2021.0141, KAW 2022.0327), Swedish Research Council (2022-01661), Natural Sciences and Engineering Research Council of Canada (RGPIN-2019-06824), and NIH/NIDCR (R01DE032712). Salary support for JCW was provided by the Fonds de recherche du Québec – Santé (FRQS), the Canadian Allergy, Asthma, and Immunology Foundation, Asthma Canada (CAAIF), and CIHR (Institute of Circulatory and Respiratory Health).

REFERENCES

1. Connolly, R. *et al.* Mortality attributable to PM2.5 from wildland fires in California from 2008 to 2018. *Science advances* **10,** eadl1252; 10.1126/sciadv.adl1252 (2024).
2. Ray, A. & Kolls, J. K. Neutrophilic Inflammation in Asthma and Association with Disease Severity. *Trends in immunology* **38,** 942–954; 10.1016/j.it.2017.07.003 (2017).
3. Jatakanon, A. *et al.* Neutrophilic inflammation in severe persistent asthma. *American journal of respiratory and critical care medicine* **160,** 1532–1539; 10.1164/ajrccm.160.5.9806170 (1999).
4. Talbot, S., Foster, S. L. & Woolf, C. J. Neuroimmunity: Physiology and Pathology. *Annual review of immunology* **34,** 421–447; 10.1146/annurev-immunol-041015-055340 (2016).
5. Foster, S. L., Talbot, S. & Woolf, C. J. CNS injury: IL-33 sounds the alarm. *Immunity* **42,** 403–405; 10.1016/j.immuni.2015.02.019 (2015).
6. Michoud, F. *et al.* Epineural optogenetic activation of nociceptors initiates and amplifies inflammation. *Nature biotechnology* **39,** 179–185; 10.1038/s41587-020-0673-2 (2021).
7. Bin, N.-R. *et al.* An airway-to-brain sensory pathway mediates influenza-induced sickness. *Nature* **615,** 660–667; 10.1038/s41586-023-05796-0 (2023).
8. Lai, N. Y. *et al.* Gut-Innervating Nociceptor Neurons Regulate Peyer's Patch Microfold Cells and SFB Levels to Mediate Salmonella Host Defense. *Cell* **180,** 33-49.e22; 10.1016/j.cell.2019.11.014 (2020).
9. Cohen, J. A. *et al.* Cutaneous TRPV1+ Neurons Trigger Protective Innate Type 17 Anticipatory Immunity. *Cell* **178,** 919-932.e14; 10.1016/j.cell.2019.06.022 (2019).
10. Perner, C. *et al.* Substance P Release by Sensory Neurons Triggers Dendritic Cell Migration and Initiates the Type-2 Immune Response to Allergens. *Immunity* **53,** 1063-1077.e7; 10.1016/j.immuni.2020.10.001 (2020).
11. Hanč, P. *et al.* Multimodal control of dendritic cell functions by nociceptors. *Science (New York, N.Y.)* **379,** eabm5658; 10.1126/science.abm5658 (2023).
12. Chiu, I. M. *et al.* Bacteria activate sensory neurons that modulate pain and inflammation. *Nature* **501,** 52–57; 10.1038/nature12479 (2013).
13. Balood, M. *et al.* Nociceptor neurons affect cancer immunosurveillance. *Nature* **611,** 405–412; 10.1038/s41586-022-05374-w (2022).
14. Restaino, A. C. *et al.* Functional neuronal circuits promote disease progression in cancer. *Science advances* **9,** eade4443; 10.1126/sciadv.ade4443 (2023).
15. Barr, J. *et al.* Tumor-infiltrating nerves functionally alter brain circuits and modulate behavior in a male mouse model of head-and-neck cancer. *bioRxiv : the preprint server for biology*; 10.1101/2023.10.18.562990 (2024).
16. Amit, M. *et al.* Next Directions in the Neuroscience of Cancers Arising outside the CNS. *Cancer discovery* **14,** 669–673; 10.1158/2159-8290.CD-23-1495 (2024).
17. Foster, S. L., Seehus, C. R., Woolf, C. J. & Talbot, S. Sense and Immunity: Context-Dependent Neuro-Immune Interplay. *Frontiers in immunology* **8,** 1463; 10.3389/fimmu.2017.01463 (2017).
18. Talbot, S. *et al.* Silencing Nociceptor Neurons Reduces Allergic Airway Inflammation. *Neuron* **87,** 341–354; 10.1016/j.neuron.2015.06.007 (2015).
19. Tränkner, D., Hahne, N., Sugino, K., Hoon, M. A. & Zuker, C. Population of sensory neurons essential for asthmatic hyperreactivity of inflamed airways. *Proceedings of the National Academy of Sciences of the United States of America* **111,** 11515–11520; 10.1073/pnas.1411032111 (2014).
20. Talbot, S. *et al.* Vagal sensory neurons drive mucous cell metaplasia. *The Journal of allergy and clinical immunology* **145,** 1693-1696.e4; 10.1016/j.jaci.2020.01.003 (2020).
21. Yang, D. *et al.* Nociceptor neurons direct goblet cells via a CGRP-RAMP1 axis to drive mucus production and gut barrier protection. *Cell* **185,** 4190-4205.e25; 10.1016/j.cell.2022.09.024 (2022).
22. Crosson, T. *et al.* FcεR1-expressing nociceptors trigger allergic airway inflammation. *The Journal of allergy and clinical immunology* **147,** 2330–2342; 10.1016/j.jaci.2020.12.644 (2021).

23. Bersellini Farinotti, A. *et al.* Cartilage-binding antibodies induce pain through immune complex-mediated activation of neurons. *The Journal of experimental medicine* **216,** 1904–1924; 10.1084/jem.20181657 (2019).

24. Mathur, S. *et al.* Nociceptor neurons promote IgE class switch in B cells. *JCI insight* **6**; 10.1172/jci.insight.148510 (2021).

25. Tynan, A. *et al.* TRPV1 nociceptors are required to optimize antigen-specific primary antibody responses to novel antigens. *Bioelectronic medicine* **10,** 14; 10.1186/s42234-024-00145-6 (2024).

26. Crosson, T. *et al.* IL-13 promotes sensory-sympathetic neurons crosstalk in asthma. *bioRxiv,* 2023.01.26.525731; 10.1101/2023.01.26.525731 (2023).

27. Wang, J.-C. *et al.* BASOPHILS ACTIVATE PRURICEPTOR-LIKE VAGAL SENSORY NEURONS. *bioRxiv : the preprint server for biology*; 10.1101/2024.06.11.598517 (2024).

28. Voisin, T. *et al.* The CysLT2R receptor mediates leukotriene C4-driven acute and chronic itch. *Proceedings of the National Academy of Sciences of the United States of America* **118**; 10.1073/pnas.2022087118 (2021).

29. Thio, C. L.-P. *et al.* Identification of a PD-L1+Tim-1+ iNKT subset that protects against fine particulate matter-induced airway inflammation. *JCI insight* **7**; 10.1172/jci.insight.164157 (2022).

30. Tochitsky, I. *et al.* Inhibition of inflammatory pain and cough by a novel charged sodium channel blocker. *British journal of pharmacology* **178,** 3905–3923; 10.1111/bph.15531 (2021).

31. Lee, S. *et al.* Novel charged sodium and calcium channel inhibitor active against neurogenic inflammation. *eLife* **8**; 10.7554/eLife.48118 (2019).

32. Binshtok, A. M., Bean, B. P. & Woolf, C. J. Inhibition of nociceptors by TRPV1-mediated entry of impermeant sodium channel blockers. *Nature* **449,** 607–610; 10.1038/nature06191 (2007).

33. Roversi, K. *et al.* Nanophotonics Enable Targeted Photothermal Silencing of Nociceptor Neurons. *Small (Weinheim an der Bergstrasse, Germany)* **18,** e2103364; 10.1002/smll.202103364 (2022).

34. Wang, J.-C., Crosson, T. & Talbot, S. Analysis of Airway Vagal Neurons. *Methods in molecular biology (Clifton, N.J.)* **2506,** 297–314; 10.1007/978-1-0716-2364-0_21 (2022).

35. Crosson, T. & Talbot, S. Anatomical differences in nociceptor neurons sensitivity. *Bioelectronic medicine* **8,** 7; 10.1186/s42234-022-00088-w (2022).

36. Honma, Y. *et al.* Artemin is a vascular-derived neurotropic factor for developing sympathetic neurons. *Neuron* **35,** 267–282; 10.1016/s0896-6273(02)00774-2 (2002).

37. Ilieva, M. *et al.* Artemin and an Artemin-Derived Peptide, Artefin, Induce Neuronal Survival, and Differentiation Through Ret and NCAM. *Frontiers in molecular neuroscience* **12,** 47; 10.3389/fnmol.2019.00047 (2019).

38. Lippoldt, E. K., Elmes, R. R., McCoy, D. D., Knowlton, W. M. & McKemy, D. D. Artemin, a glial cell line-derived neurotrophic factor family member, induces TRPM8-dependent cold pain. *The Journal of neuroscience : the official journal of the Society for Neuroscience* **33,** 12543–12552; 10.1523/JNEUROSCI.5765-12.2013 (2013).

39. Elitt, C. M. *et al.* Artemin overexpression in skin enhances expression of TRPV1 and TRPA1 in cutaneous sensory neurons and leads to behavioral sensitivity to heat and cold. *The Journal of neuroscience : the official journal of the Society for Neuroscience* **26,** 8578–8587; 10.1523/JNEUROSCI.2185-06.2006 (2006).

40. Elitt, C. M., Malin, S. A., Koerber, H. R., Davis, B. M. & Albers, K. M. Overexpression of artemin in the tongue increases expression of TRPV1 and TRPA1 in trigeminal afferents and causes oral sensitivity to capsaicin and mustard oil. *Brain research* **1230,** 80–90; 10.1016/j.brainres.2008.06.119 (2008).

41. Kupari, J., Häring, M., Agirre, E., Castelo-Branco, G. & Ernfors, P. An Atlas of Vagal Sensory Neurons and Their Molecular Specialization. *Cell reports* **27,** 2508-2523.e4; 10.1016/j.celrep.2019.04.096 (2019).

42. Pinho-Ribeiro, F. A. *et al.* Bacteria hijack a meningeal neuroimmune axis to facilitate brain invasion. *Nature* **615,** 472–481; 10.1038/s41586-023-05753-x (2023).

43. Filtjens, J. *et al.* Nociceptive sensory neurons promote CD8 T cell responses to HSV-1 infection. *Nature communications* **12,** 2936; 10.1038/s41467-021-22841-6 (2021).

44. Kashem, S. W. *et al.* Nociceptive Sensory Fibers Drive Interleukin-23 Production from CD301b+ Dermal Dendritic Cells and Drive Protective Cutaneous Immunity. *Immunity* **43,** 515–526; 10.1016/j.immuni.2015.08.016 (2015).

45. Helme, R. D., Eglezos, A., Dandie, G. W., Andrews, P. V. & Boyd, R. L. The effect of substance P on the regional lymph node antibody response to antigenic stimulation in capsaicin-pretreated rats. *Journal of immunology (Baltimore, Md. : 1950)* **139,** 3470–3473 (1987).

46. Aguilar, D. *et al.* Sensory neurons regulate stimulus-dependent humoral immunity. *bioRxiv : the preprint server for biology*; 10.1101/2024.01.04.574231 (2024).

47. Sponchiado, M. *et al.* Overexpression of Substance P in pig airways increases MUC5AC through an NF-kβ pathway. *Physiological reports* **9,** e14749; 10.14814/phy2.14749 (2021).

48. Hanes, W. M. *et al.* Neuronal Circuits Modulate Antigen Flow Through Lymph Nodes. *Bioelectronic medicine* **3,** 18–28; 10.15424/bioelectronmed.2016.00001 (2016).

49. Huang, S. *et al.* Lymph nodes are innervated by a unique population of sensory neurons with immunomodulatory potential. *Cell* **184,** 441-459.e25; 10.1016/j.cell.2020.11.028 (2021).

50. Riol-Blanco, L. *et al.* Nociceptive sensory neurons drive interleukin-23-mediated psoriasiform skin inflammation. *Nature* **510,** 157–161; 10.1038/nature13199 (2014).

51. Klose, C. S. N. *et al.* The neuropeptide neuromedin U stimulates innate lymphoid cells and type 2 inflammation. *Nature* **549,** 282–286; 10.1038/nature23676 (2017).

52. Cardoso, V. *et al.* Neuronal regulation of type 2 innate lymphoid cells via neuromedin U. *Nature* **549,** 277–281; 10.1038/nature23469 (2017).

53. Wallrapp, A. *et al.* The neuropeptide NMU amplifies ILC2-driven allergic lung inflammation. *Nature* **549,** 351–356; 10.1038/nature24029 (2017).

54. Nussbaum, J. C. *et al.* Type 2 innate lymphoid cells control eosinophil homeostasis. *Nature* **502,** 245–248; 10.1038/nature12526 (2013).

55. Sui, P. *et al.* Pulmonary neuroendocrine cells amplify allergic asthma responses. *Science (New York, N.Y.)* **360**; 10.1126/science.aan8546 (2018).

56. Ike, E., Kawano, T., Takahashi, K., Miyasaka, T. & Takahashi, T. Calcitonin Gene-Related peptide receptor antagonist suppresses allergic asthma responses via downregulation of group 2 innate lymphoid cells in mice. *International immunopharmacology* **122,** 110608; 10.1016/j.intimp.2023.110608 (2023).

57. Wallrapp, A. *et al.* Calcitonin Gene-Related Peptide Negatively Regulates Alarmin-Driven Type 2 Innate Lymphoid Cell Responses. *Immunity* **51,** 709-723.e6; 10.1016/j.immuni.2019.09.005 (2019).

58. Huang, C. *et al.* TRPV1+ neurons alter Staphylococcus aureus skin infection outcomes by affecting macrophage polarization and neutrophil recruitment. *BMC immunology* **24,** 55; 10.1186/s12865-023-00584-x (2023).

59. Baral, P. *et al.* Nociceptor sensory neurons suppress neutrophil and γδ T cell responses in bacterial lung infections and lethal pneumonia. *Nature medicine* **24,** 417–426; 10.1038/nm.4501 (2018).

60. Bissonnette, R., Stein Gold, L., Rubenstein, D. S., Tallman, A. M. & Armstrong, A. Tapinarof in the treatment of psoriasis: A review of the unique mechanism of action of a novel therapeutic aryl hydrocarbon receptor-modulating agent. *Journal of the American Academy of Dermatology* **84,** 1059–1067; 10.1016/j.jaad.2020.10.085 (2021).

61. Di Meglio, P. *et al.* Activation of the aryl hydrocarbon receptor dampens the severity of inflammatory skin conditions. *Immunity* **40,** 989–1001; 10.1016/j.immuni.2014.04.019 (2014).

62. Wang, Y. *et al.* Aryl hydrocarbon receptor restricts axon regeneration of DRG neurons in response to injury. *bioRxiv : the preprint server for biology*; 10.1101/2023.11.04.565649 (2023).

63. Barroso, A., Mahler, J. V., Fonseca-Castro, P. H. & Quintana, F. J. The aryl hydrocarbon receptor and the gut-brain axis. *Cellular & molecular immunology* **18,** 259–268; 10.1038/s41423-020-00585-5 (2021).

64. Neupane, A. S. *et al.* Patrolling Alveolar Macrophages Conceal Bacteria from the Immune System to Maintain Homeostasis. *Cell* **183,** 110-125.e11; 10.1016/j.cell.2020.08.020 (2020).

65. Wilson, S. R. *et al.* The epithelial cell-derived atopic dermatitis cytokine TSLP activates neurons to induce itch. *Cell* **155,** 285–295; 10.1016/j.cell.2013.08.057 (2013).

66. Caceres, A. I. *et al.* A sensory neuronal ion channel essential for airway inflammation and hyperreactivity in asthma. *Proceedings of the National Academy of Sciences of the United States of America* **106,** 9099–9104; 10.1073/pnas.0900591106 (2009).

67. Bessac, B. F. *et al.* Transient receptor potential ankyrin 1 antagonists block the noxious effects of toxic industrial isocyanates and tear gases. *FASEB journal : official publication of the Federation of American Societies for Experimental Biology* **23,** 1102–1114; 10.1096/fj.08-117812 (2009).

68. Balestrini, A. *et al.* A TRPA1 inhibitor suppresses neurogenic inflammation and airway contraction for asthma treatment. *The Journal of experimental medicine* **218**; 10.1084/jem.20201637 (2021).

69. Yeo, H. *et al.* The EGR1-Artemin Axis in Keratinocytes Enhances the Innervation of Epidermal Sensory Neurons during Skin Inflammation Induced by House Dust Mite Extract from Dermatophagoidesfarinae. *The Journal of investigative dermatology* **144,** 1817-1828.e17; 10.1016/j.jid.2024.01.017 (2024).

70. Heng, T. S. P. & Painter, M. W. The Immunological Genome Project: networks of gene expression in immune cells. *Nature immunology* **9,** 1091–1094; 10.1038/ni1008-1091 (2008).

71. Gupta, S. *et al.* Navigating the blurred path of mixed neuroimmune signaling. *The Journal of allergy and clinical immunology* **153,** 924–938; 10.1016/j.jaci.2024.02.006 (2024).

72. Roversi, K. *et al.* Neuro-Immunity and Gut Dysbiosis Drive Parkinson's Disease-Induced Pain. *Frontiers in immunology* **12,** 759679; 10.3389/fimmu.2021.759679 (2021).

73. Eichwald, T. & Talbot, S. Neuro-Immunity Controls Obesity-Induced Pain. *Frontiers in human neuroscience* **14,** 181; 10.3389/fnhum.2020.00181 (2020).

74. Rajchgot, T. *et al.* Neurons and Microglia; A Sickly-Sweet Duo in Diabetic Pain Neuropathy. *Frontiers in neuroscience* **13,** 25; 10.3389/fnins.2019.00025 (2019).

75. Deng, L. *et al.* S. aureus drives itch and scratch-induced skin damage through a V8 protease-PAR1 axis. *Cell* **186,** 5375-5393.e25; 10.1016/j.cell.2023.10.019 (2023).

76. Ruhl, C. R. *et al.* Mycobacterium tuberculosis Sulfolipid-1 Activates Nociceptive Neurons and Induces Cough. *Cell* **181,** 293-305.e11; 10.1016/j.cell.2020.02.026 (2020).

77. Azimi, E. *et al.* Substance P activates Mas-related G protein-coupled receptors to induce itch. *The Journal of allergy and clinical immunology* **140,** 447-453.e3; 10.1016/j.jaci.2016.12.980 (2017).

78. Azimi, E. *et al.* Dual action of neurokinin-1 antagonists on Mas-related GPCRs. *JCI insight* **1,** e89362; 10.1172/jci.insight.89362 (2016).

79. Chiu, I. M., Hehn, C. A. von & Woolf, C. J. Neurogenic inflammation and the peripheral nervous system in host defense and immunopathology. *Nature neuroscience* **15,** 1063–1067; 10.1038/nn.3144 (2012).

80. Jackson, D. J. *et al.* Reduction of daily maintenance inhaled corticosteroids in patients with severe eosinophilic asthma treated with benralizumab (SHAMAL): a randomised, multicentre, open-label, phase 4 study. *Lancet (London, England)* **403,** 271–281; 10.1016/S0140-6736(23)02284-5 (2024).